A Method of Measuring Acoustic Wave Attenuation in the Laboratory

by

X.M. Tang, M.N. Toksöz, P. Tarif, and R.H. Wilkens

Earth Resources Laboratory
Department of Earth, Atmospheric, and Planetary Sciences
Massachusetts Institute of Technology
Cambridge, MA 02139

ABSTRACT

The measurement of attenuation is performed by directly determining the attenuation operator (or the impulse response of the medium) in the time domain. In this way, it is possible to separate the attenuation operator from other non-attenuation effects, e.g. reflections. The Wiener filtering technique, or the damped least-squares, is used to calculate the attenuation operator. For the damped least squares, we have corrected for the effect due to the addition of the damping constant using a perturbation method. Numerical tests are carried out to illustrate the technique.

The geometric beam spreading of ultrasonic waves generated by a source of finite size can strongly affect the result of attenuation measurements. Corrections are made by equating the received signal to the average pressure over the receiver surface.

The technique is used to measure ultrasonic attenuation in water, glycerol and mud. The measurement in water offers a test of the corrections made for the geometric beam spreading. The measurement in glycerol and mud shows that, in the frequency range of 0.2–1.5 MHz, the attenuation of glycerol increases rapidly with frequency, whereas the attenuation of mud is proportional to frequency, exhibiting a constant Q behavior. The measurements show that the technique used here is an effective approach to the measurement of attenuation.

INTRODUCTION

Accurate measurement of intrinsic attenuation is difficult to obtain because, in addition to intrinsic damping, factors such as geometric spreading, reflections, scattering may strongly affect propagating waves. For this reason, we often speak of the measured attenuation as "apparent attenuation" and, in certain cases, this apparent attenuation significantly differs from the intrinsic attenuation which interests us. Thus, in order to obtain the true attenuation, it is necessary to correct for these other effects.

A major effect on the attenuation measurement in the laboratory is the geometric beam spreading of waves generated by a source of finite size. In the laboratory, most ultrasonic measurements are performed at distances close to the Fresnel zone, where the diffraction effect strongly distorts propagating waves and changes their frequency content. ·This effect, if uncorrected, leads to erroneous results, and it must be taken into account to obtain reasonable estimates of attenuation.

In the laboratory, attenuation can be measured using a pulse transmission technique (Toksöz et al., 1978), in which the spectra of two separate signals are compared, and the attenuation is found from the slope of the natural logarithm of their spectral ratio. This is commonly referred to as the "spectral ratio method" and is widely used both in the laboratory and in the field. However, signals may be contaminated by noise (especially in the field), or they may be mixed with extra arrivals, e.g. reflections from side walls, boundaries in the laboratory. In practice, signals are truncated to remove these extra arrivals. But truncation usually affects the wave spectra particularly when the removed parts still contain a significant portion of the signal. Therefore, when later parts of signals are mixed with extra arrivals, truncated or not, the wave spectra will be affected to a certain extent. In this study, we present a solution to this problem by determining the attenuation operator in the time domain.

In the following section, we determine the attenuation operator by a damped least-squares (or Wiener) deconvolution, then correct the damping effect using a perturbation technique, and give some numerical examples. Next, we describe how to correct for the diffraction effects in the attenuation measurement. Finally, we apply the technique to the actual measurement of attenuation and present some results.

DETERMINATION OF ATTENUATION OPERATOR USING WIENER FILTERING

Given a signal recorded at two different locations from a single source, we want to calculate the inter-receiver medium transfer function (corresponding to the medium

impulse response or the attenuation operator). Figure 1 illustrates the problem in the time and frequency domain where the input signal at location 1 is convolved with the inter-receiver attenuation operator to produce the output at location 2. As a result, the medium transfer function is given by the following spectral ratio

$$H(\omega) = \frac{F_2(\omega)}{F_1(\omega)} \tag{1}$$

where ω is the angular frequency, $F(\omega)$ is the signal spectrum, and subscripts 1 and 2 refer to the two locations of the receivers at distances z_1 and z_2 ($> z_1$) from the source, respectively. Let us now express equation (1) using its time domain representation

$$f_2(t) = f_1(t) * h(t) \tag{2}$$

where t is time, $f(t)$ and $h(t)$ are the inverse Fourier transform of $F(\omega)$ and $H(\omega)$, respectively, and $*$ denotes convolution. In order to find the filter coefficients of $h(t)$, we solve equation (2) using Wiener deconvolution (Peacock and Treitel, 1969; Taylor and Toksöz, 1982). Using discretized signals $f_1(t)$ and $f_2(t)$ and applying the least-squares technique, we can determine the Wiener filter $h(t)$ via the following equation

$$Ah = g \tag{3}$$

where h is a vector representing the filter, A is a Toeplitz form matrix whose elements are the autocorrelation of $f_1(t)$, and g is a vector determined by the cross-correlation of $f_1(t)$ with $f_2(t)$. Because the autocorrelation matrix A in equation (3) is in Toeplitz form, this equation can be solved efficiently using Levinson recursion (Wiener, 1949; Aki and Richards, 1980) with a minimum of computer storage and the least computational time. However, numerical instabilities often occur when the filter length is large. To stabilize the numerical system, we add a constant θ^2 to the diagonals of the matrix A, and equation (3) may now be written as

$$(A + \theta^2 I)h = g \tag{4}$$

where I is the unit matrix. This method is essentially the damped least-squares technique.

Although the addition of θ^2 stabilizes the system, the filter estimate is altered, and corrections are needed to recover the true filter values, especially when θ^2 is not small. Taylor and Toksöz (1982) presented a method for making the correction in the frequency domain, in which the altered spectral estimate of $h(t)$ was multiplied by $(A(\omega) + \theta^2)/A(\omega)$, and $A(\omega)$ was estimated by taking a Fourier transform of the autocorrelation function. However, as will be shown below, this correction may be made directly in the time domain.

Let h_1 denote the solution of equation (4), which is the altered estimate of h, and h_2 the difference between the true and the altered estimate of h

$$h = h_1 + h_2 \tag{5}$$

(a)   input wavelet   attenuation operator   attenuated wavelet

(b)

$$F_1(\omega) \;\rightarrow\; \boxed{H(\omega)} \;\rightarrow\; F_2(\omega)$$
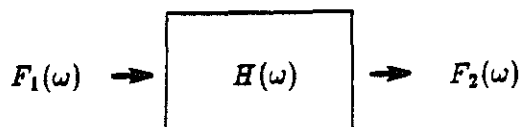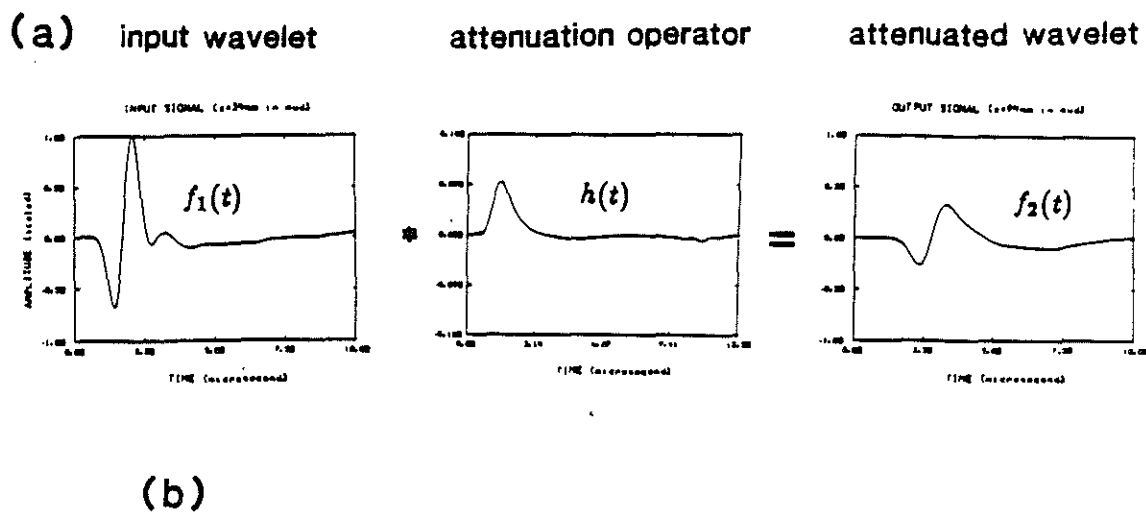
Figure 1: Schematic formulation of the wave attenuation problem. (a) Wavelet at location nearest to the source is convolved with the inter-receiver attenuation operator to give the output wavelet at the location furthest from the source. (b) Frequency domain representation of (a).

Subtracting equation (4) from equation (3), we then have

$$Ah_2 = \theta^2 h_1 \tag{6}$$

Note that equation (6) has the same form as equation (3), where h and g have been replaced by h_2 and $\theta^2 h_1$, respectively. Once h_2 is found by solving equation (6), the true filter estimate is given by equation (5). Taking the Fourier transform of equations (5) and (6), we can easily show that

$$H(\omega) = H_1(\omega)\frac{A(\omega) + \theta^2}{A(\omega)} \tag{7}$$

where $H_1(\omega)$, corresponding to h_1, is the altered estimate of the transfer function, and $A(\omega)$ is the Fourier transform of the autocorrelation function, as explained by Taylor and Toksöz (1982). At this stage, our method of correction is essentially the time domain equivalence of the Taylor and Toksöz method. However, because of the numerical instability of the matrix A in equation (6), the addition of the damping constant θ^2 is again needed to calculate h_2, and the result is the altered estimate of h_2. Since Levinson recursion requires the least computational time to solve equations like equation (4), the same procedure can be carried out repeatedly, as follows

$$(A + \theta^2 I)h_n = \theta^2 h_{n-1}, \quad n = 2, 3, \cdots \tag{8}$$

and each solution of equation (8) is added up to approach the true filter estimate

$$h = h_1 + h_2 + \cdots + h_n + \cdots \tag{9}$$

The same procedure can be repeated as many times as necessary until the n-th estimate h_n is close to zero. In practice, three or four repetitions are sufficient to return the true estimate of the filter. This method of correction is essentially the perturbation technique. The interesting point to note is that we try to recover the unperturbed solution using perturbed solutions.

The damping constant θ^2 can be selected as follows: We start the Levinson recursion with $\theta^2 = 0$. If numerical instabilities occur, we add a small θ^2, typically $0.05a_0$, (where a_0 is the autocorrelation at zero lag, or the diagonal element of the matrix A), and repeat the recursion; if the added θ^2 is not sufficient to stabilize the system, we increase θ^2 until the stability is achieved. Doing so, the smallest value of θ^2 needed to stabilize the system is found and is used in equation (8) for later corrections.

The following numerical tests are carried out to illustrate this technique.

1. Correction for the effect due to the damping constant.

2. Separation of attenuation operator and extra arrivals.

3. Separation of attenuation operator and truncation effects.

We first let

$$f_1(t) = t^{\alpha} e^{-\beta t} sin(\gamma t) \tag{10}$$

where α, β, and γ are constants. We then convolve the given $f_1(t)$ with a constant Q attenuation operator (Kjartansson, 1979) to produce the output signal $f_2(t)$. With $f_1(t)$ and $f_2(t)$ at hand, we reverse the procedure and apply the above technique to derive the attenuation operator. The comparison of the recovered operator with the test operator offers a test for the technique.

For test case (1), the filter length is 150, and the damping constant is $0.3a_0$. The input and output signals $f_1(t)$ and $f_2(t)$ are shown in Figure 2. Figure 3a shows the altered pulse estimate and its two successive corrections calculated using equation (8). With four corrections (only the first two are shown in Figure 3a, the other two being small), the corrected pulse is very close to the test pulse, as can be seen in Figure 3b.

For test case (2), $f_1(t)$ and $f_2(t)$ both contain a tail which is added to simulate extra arrivals (Figure 4); these tails are also generated using equation (10). The two signals are then processed using Wiener filtering, and the recovered attenuation operator is shown in Figure 5, together with a tail due to the added extra arrivals. Fortunately, this tail is almost separated from the pulse; by truncating this tail, the main feature of the test attenuation operator is recovered.

For test case (3), the unwanted tails are removed by truncating the signals at the time point where the later arrival appears (indicated by an arrow in Figure 4). Note that while most of the energy remains in the truncated signals, a small amount is lost because of the truncation. The truncated signals $f_1(t)$ and $f_2(t)$ are then processed using Wiener filtering, and the result is given in Figure 6. The recovered pulse exhibits some effect which is obviously due to the truncation, for the onset of this effect (indicated by an arrow in Figure 6) corresponds to the time point where $f_1(t)$ is truncated. From this figure we can see that because the pulse is separated from the truncation effects, the recovered pulse is again close to the test pulse.

It is worthwhile to note that in both cases (2) and (3), either the arrival time difference between the signal itself and the extra arrivals or the truncated signal duration is longer than the duration of the attenuation operator. This practically determines the extent to which the effects due to intrinsic attenuation are separable from the effects due to extra arrivals.
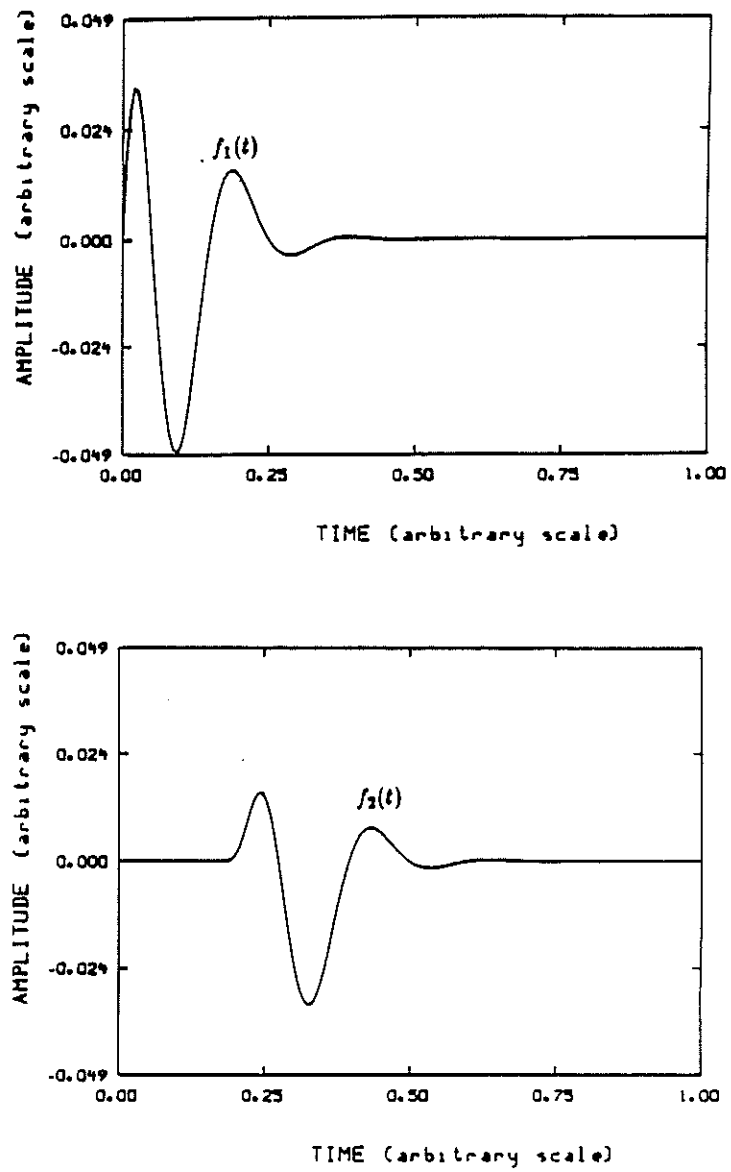
Figure 2: Input and output signals used to calculate the attenuation operator
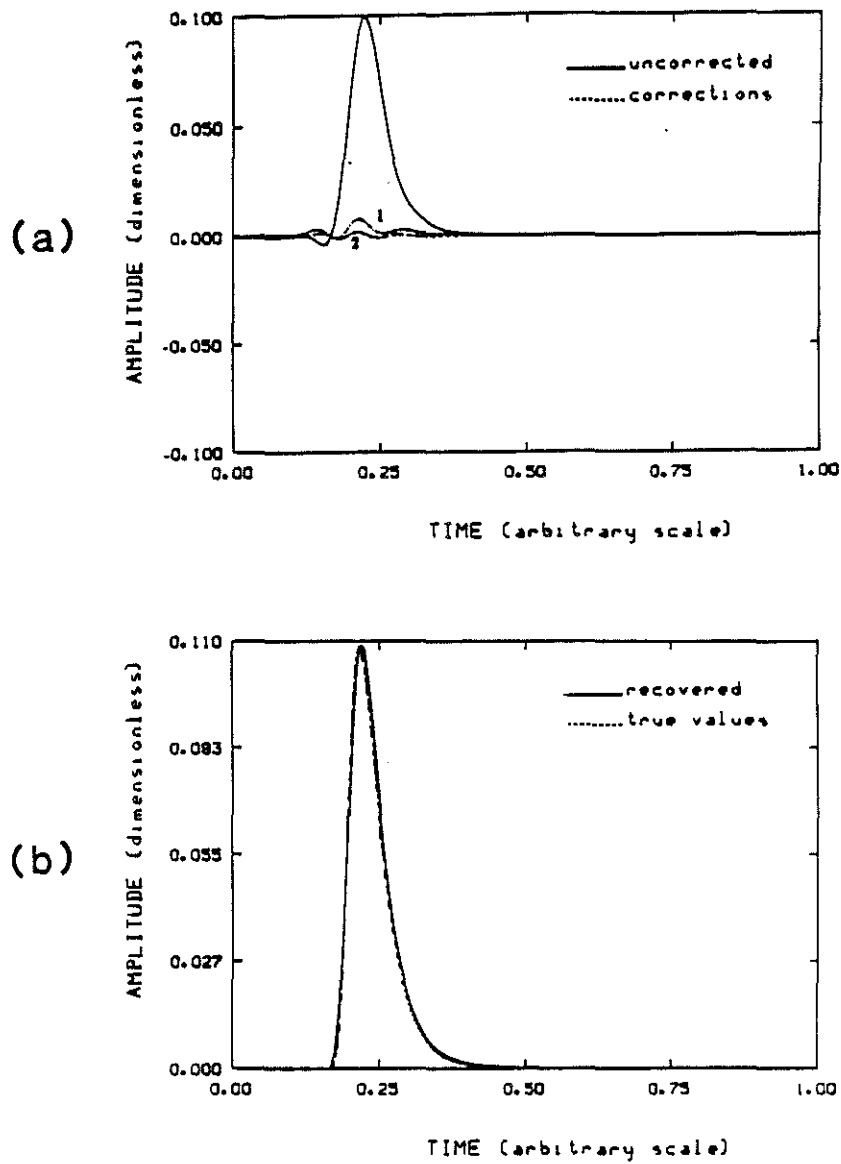
Tang et al.

Figure 3: (a) The altered estimate of the attenuation operator and its first and second order corrections (indicated by 1 and 2). (b) Comparison of the corrected pulse with the test pulse.
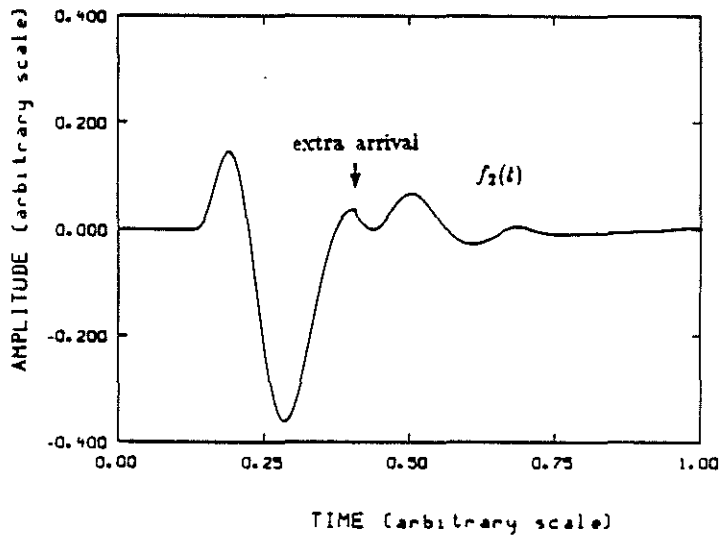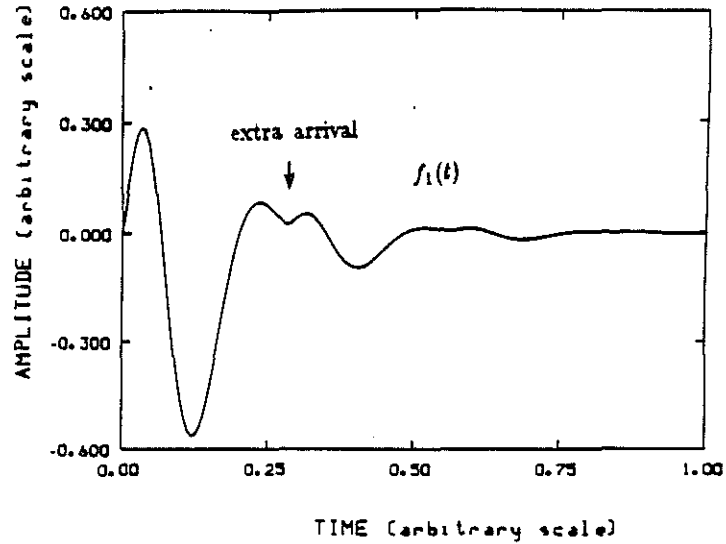
Figure 4: Input and output signals added with tails to simulate extra arrivals.
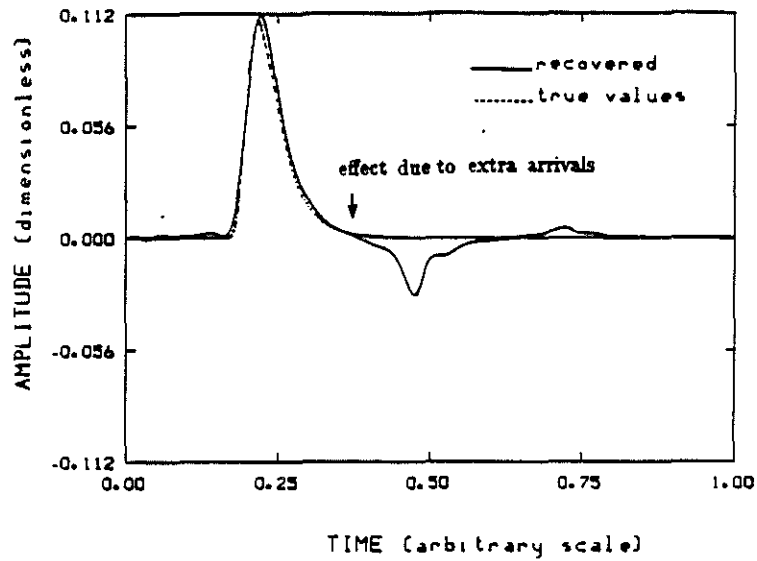
Tang et al.

Figure 5: The recovered pulse with effects due to extra arrivals and its comparison with the test pulse.
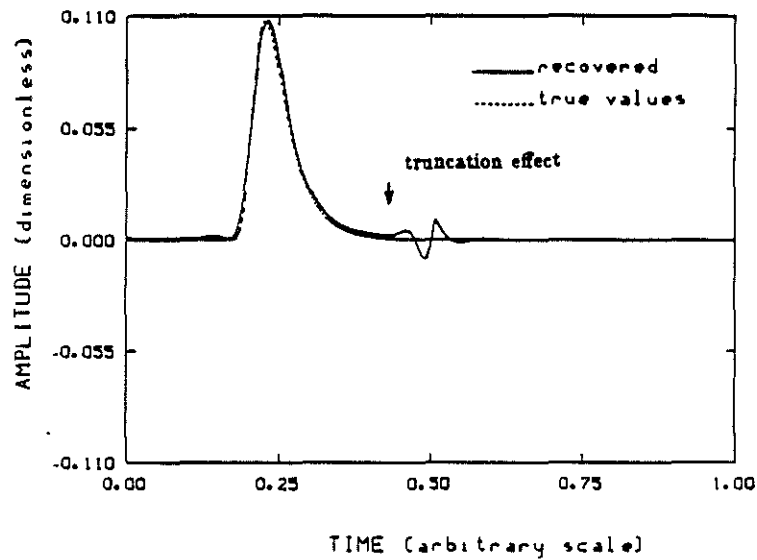

Figure 6: The recovered pulse having truncation effects and its comparison with the test pulse.

CORRECTION FOR GEOMETRIC BEAM SPREADING

During ultrasonic measurements executed in the laboratory, the main source of error is due to the diffraction phenomenon, which arises from the finite dimensions of transducers compared with the wavelength. As an example, two measurements are made in water with the source and receiver transducers coaxially aligned. Both transducers have a radius of $7mm$ and a center frequency of 0.8 MHz. Receiver distances from the source are $14mm$ and $94mm$. The measured wave spectra are shown in Figure 7. We can see from the normalized spectra in this figure that the spectrum furthest from the source has relatively less low frequency content. Since attenuation in water is negligible, the observed phenomenon is mainly due to the diffraction effects of the wave field. Consequently, in the attenuation measurement the wave spectra will be affected by both attenuation and diffraction; the latter effect has to be corrected before any reasonable estimate of attenuation can be obtained.

Let us consider cylindrical coordinates with the origin of the z axis at the center of the source transducer, and the radial coordinate r perpendicular to the z axis. If the velocity amplitude at the source surface is $v_0(t)$, then the pressure at the field point (r, z) is given by the following convolution (Harris, 1981).

$$p(r, z; t) = \rho v_0(t) * \frac{d}{dt}[h(r, z; t)] \tag{11}$$

where ρ is the density of the propagation medium, and $h(r, z; t)$ is the spatial impulse response (Harris, 1981). For pressure signals, the time derivative of $h(r, z; t)$ acts like an operator. Because we are dealing with pressure signals, let us call the time derivative of $h(r, z; t)$ the spatial pressure impulse response $h_p(r, z; t)$

$$h_p(r, z; t) = \frac{d}{dt}[h(r, z; t)] \tag{12}$$

In dealing with pressure signals received by a transducer, it is common practice to equate them to the average pressure over the receiver surface (Gitis and Khimunin, 1969). In our case, the receiver and the source have the same geometry, thus the average pressure $\langle p \rangle_{AV}$ is given by

$$\langle p \rangle_{AV}(z; t \ or \ \omega) = \frac{1}{\pi a^2} \int_0^{2\pi} d\phi \int_0^a p(r, z; t \ or \ \omega) r dr \tag{13}$$

where a is the radius of the transducer. Williams (1951) was the first to derive an integral expression for the averaged acoustic field over a 'measurement circle' of radius a. This expression, in terms of the pressure transfer function (corresponding to h_p), may be written as

$$\langle H_p \rangle_{AV}(z, \omega) = \frac{\omega}{k} e^{-ikz} - \frac{4\omega}{\pi k} \int_0^{2\pi} exp\left\{-ik\sqrt{z^2 + 4a^2 cos^2\theta}\right\} sin^2\theta d\theta \tag{14}$$
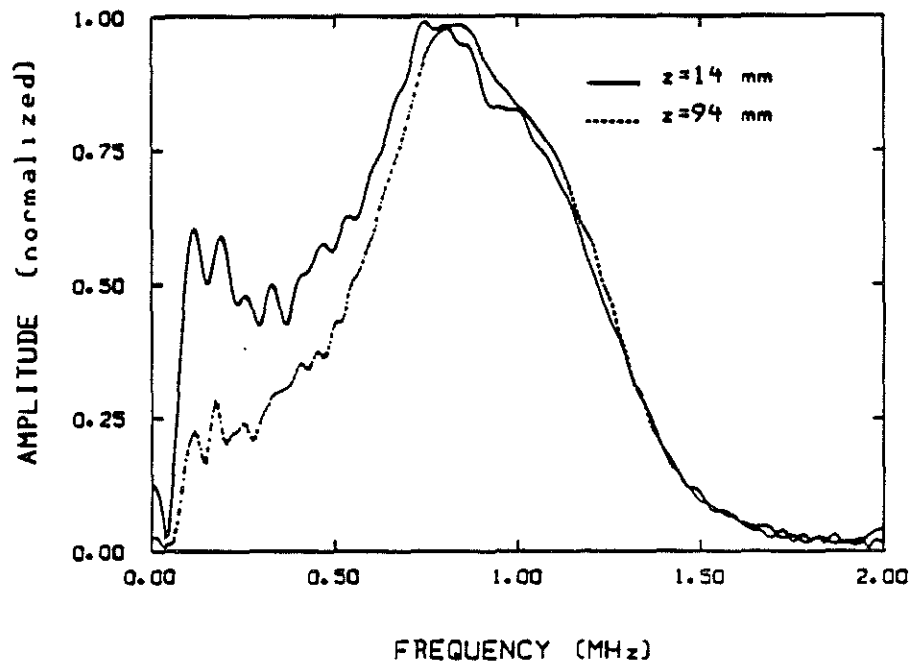
Figure 7: Normalized wave spectra of two transducer signals received at 14*mm* and 94*mm* from the source, respectively. Note that the spectrum furthest from the source has less low frequency content than that of the nearest one.

where k is the wavenumber of the medium. By taking the inverse Fourier transform of equation (14), we can readily derive the averaged spatial pressure impulse response as follows

$$\langle h_p \rangle_{AV}(z,t) = c\delta(t - \frac{z}{c}) - \frac{c^3 t}{\pi a^2}\sqrt{\frac{4a^2 + z^2 - c^2 t^2}{c^2 t^2 - z^2}}u(ct - z)u(\sqrt{z^2 + 4a^2} - ct) \qquad (15)$$

where $\delta(t)$ represents the delta function, c is phase velocity, and $u(t)$ is the step function. A few remarks will help to explain how the average spatial response operates on the received signals. The first term in equation (15) is the plane wave pulse unaffected by the averaging operation, while the second negative term is called the edge wave (Harris, 1981). The edge pulse duration is $\sqrt{4a^2 + z^2}/c - z/c$. Like the first term, the integral of the edge term over time (or the area covered by the edge term) is a constant for any z. Near the source ($z \to 0$), the edge wave duration is the longest, and its amplitude is the smallest. As z increases, its duration decreases and amplitude increases. When z is very large, it tends to be close to a delta function, and the average spatial pressure impulse response approaches $\delta'(t)$, the time derivative of the delta function. When a source signal is convolved with $\delta'(t)$ (see equation (11)), it results in the time differentiation of the signal itself, which tends to remove the low frequency portion of the signal. Thus we see that while waves propagate away from the transducer source, they gradually lose their low frequency content because of the diffraction effects. This is indeed what we have seen in Figure 7.

With the use of equation (14) the source spectrum can now be restored from the measured wave spectrum. Because corrections are to be made for the whole wave spectrum, equation (14) must be evaluated from low to high frequencies. Although the integral in this equation can be calculated using numerical methods, the computation turns out to be very time consuming, especially for high frequencies. Therefore, we turn our attention to the use of approximate expressions. In his paper, Williams (1951) also derived a lengthy approximate solution of equation (14) by expanding the exponential function in series (see his equation (28)). Doing so, he imposed the following condition

$$z/a > (ka)^{\frac{1}{3}} \qquad (16)$$

Unfortunately, this condition breaks down easily at high frequencies and greatly restricts the usefulness of his formula. However, when inequality (16) is satisfied, his approximate solution is accurate. Later, Bass (1958) derived another approximate solution of equation (14) using a series expansion of the $sin^2\theta$ function. His expression, in terms of the pressure transfer function, is given as

$$\langle H_p \rangle_{AV}(z,\omega) \doteq \frac{\omega}{k}e^{-ikz}\left\{ 1 - (1 - \frac{\xi^2}{2k^2 a^2})[J_0(\xi) + iJ_1(\xi)]e^{-i\xi} - \frac{\xi^2}{k^2 a^2}\left[\frac{iJ_1(\xi)}{\xi}\right]e^{-i\xi}\right\}$$

$$(17)$$

where

$$\xi = \frac{k}{2}(\sqrt{4a^2 + z^2} - z) \qquad (18)$$

is a dimensionless frequency, and J_0 and J_1 are ordinary Bessel functions. Compared with Williams' formula, Bass' expression is simpler, more general, and most importantly, valid for almost all frequencies. This last advantage suits our purpose of making corrections for the whole wave spectrum. However, it should be noted that equation (17) deviates from the true values near the zero frequency. It can be shown from equation (14) that the average transfer function has a true value of zero at zero frequency, while equation (17) gives a non-zero value of

$$\langle H_p \rangle_{AV}(z, \omega = 0) \doteq \frac{c(1-i)}{2} \frac{(\sqrt{4a^2 + z^2} - z)^2}{4a^2} \tag{19}$$

For small z, this error can be important. However, this problem can be solved by evaluating equation (14) either numerically, or using Williams' formula near the zero frequency.

In an attenuating medium, the effects of intrinsic attenuation are taken into account by introducing a complex wavenumber k into equation (14) or (17). We notice that the medium transfer function from which we want to derive attenuation and the spatial transfer function interact in a complicated way. However, we will show that this poses no practical problem. Let us write k as

$$k = \kappa - i\alpha \tag{20}$$

where $\kappa = \omega/c$, and the attenuation coefficient α is given by

$$\alpha = \frac{\omega}{2Qc} \tag{21}$$

where Q is the quality factor of the medium. The medium transfer function e^{-ikz} is separated from the spatial terms, as can be seen from equation (17), but the spatial terms still contain the effects of attenuation which are to be evaluated. Assuming that Q is independent of frequency (i.e., α is effectively proportional to frequency), we now evaluate the effects of attenuation by setting $Q = 30$ (fairly strong attenuation) and $Q = \infty$ (no attenuation), and compare the results obtained from equation (17) (note that the term e^{-ikz} is incorporated into the medium transfer function, thus it is not involved in the calculation, and near the zero frequency Williams' (1951) equation (28) is used). Figure 8a shows the amplitude spectra of the spatial transfer function with and without attenuation. At low frequencies where the attenuation effects are weak, the two curves are identical; at high frequencies, they show a small systematic difference. As will be shown bellow, this small difference can be ignored when the ratio of transfer functions is used.

Let $F(\omega, z_1)$ and $F(\omega, z_2)$ represent the pressure signal spectra received at z_1 and z_2, respectively, then the inter-receiver transfer function having both medium and spatial effects is given by the following spectral ratio

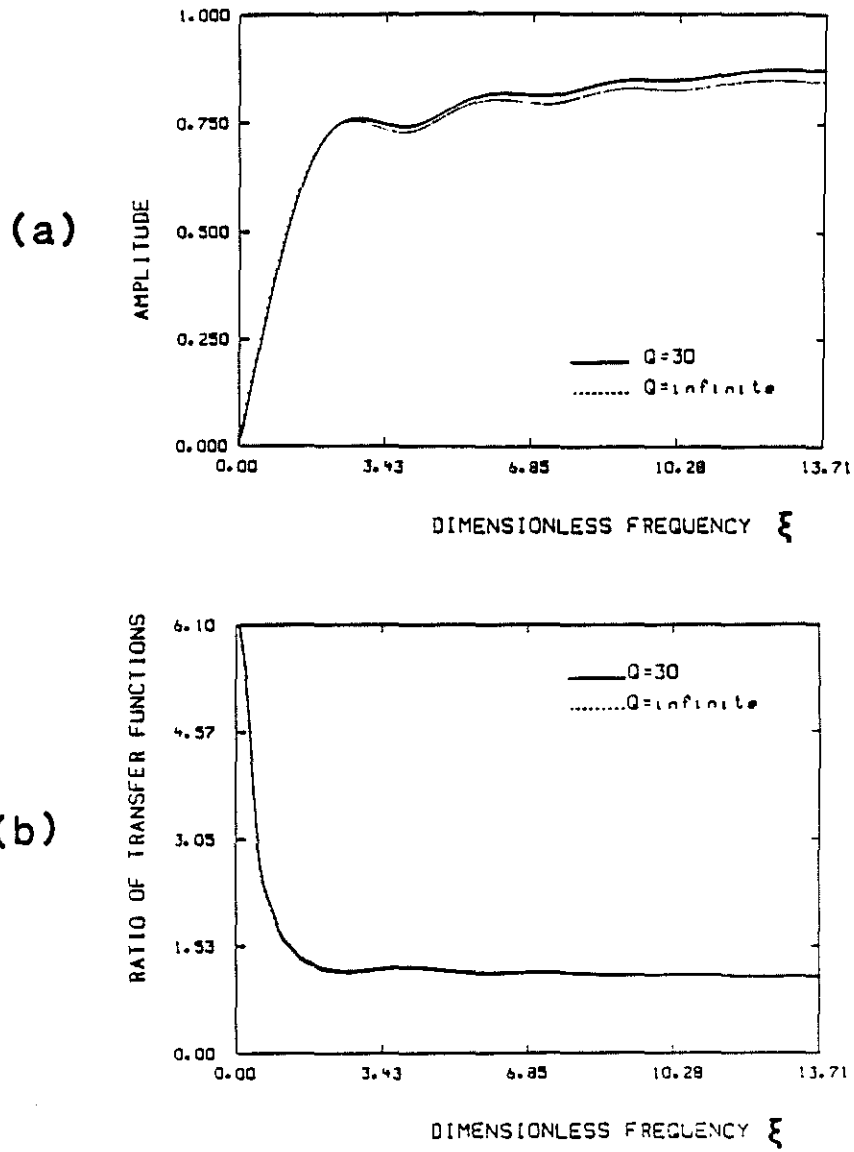$$H(\omega, z_2 - z_1) = \frac{F(\omega, z_2)}{F(\omega, z_1)} \tag{22}$$

Figure 8: (a) Comparison of amplitude spectra of the spatial transfer function with and without attenuation effects. The dimensionless frequency ξ is given by equation (18). (b) Comparison of ratios of spatial transfer functions of $z_1 = 20mm$ and $z_2 = 150mm$ with and without attenuation effects.

The inter-receiver medium transfer function $H_m = e^{-ik(z_2 - z_1)}$ can be shown to be given by

$$H_m(\omega, z_2 - z_1) = H(\omega, z_2 - z_1) \frac{\langle H_p \rangle_{AV}(k, z_1)}{\langle H_p \rangle_{AV}(k, z_2)} \qquad (23)$$

where $\langle H_p \rangle_{AV}(k, z)$ is the averaged spatial transfer function given by equation (17) (without the e^{-ikz} term), and k can be made complex to include the attenuation effect. As before, we set $Q = 30$ and $Q = \infty$, respectively. Then $\langle H_p \rangle_{AV}(k, z)$ is calculated for $z_1 = 20mm$ and $z_2 = 150mm$ to give the spectral ratio in equation (23). The spectral ratios for $Q = 30$ and $Q = \infty$ are shown in Figure 8b. To our satisfaction, spectral ratios with and without attenuation are almost identical; this is because the effects of attenuation are nearly canceled by employing the ratio of the transfer functions. Therefore, in the determination of the medium transfer function, we can feel safe to use equation (23) without making corrections for the intrinsic attenuation in the spatial transfer functions.

APPLICATION

The Wiener filtering technique, together with the corrections for the diffraction effects, is applied to the measurement of attenuation in water, glycerol, and mud under room pressure and temperature. Table 1 shows the descriptions of these three materials, as well as the attenuation data of water and glycerol available from Richardson (1962). As can be seen from Table 1, the attenuation of water is small. The attenuation of glycerol, although small at 1 MHz, increases with frequency and reaches the order of $2.3cm^{-1}$ at 10 MHz. The attenuation of the mud (water base) is to be measured in this study.

We first study the water case. We apply the Wiener deconvolution to the two signals whose normalized spectra were already shown in Figure 7, and then obtain the inter-receiver spatial pressure impulse response. From Figure 9a we see that this response does have a negative component which is due to the edge wave effect described previously. We then Fourier transform this response into the frequency domain to obtain the transfer function, from which we can calculate the attenuation coefficient α via the following

Table 16.1: Media used in measurement

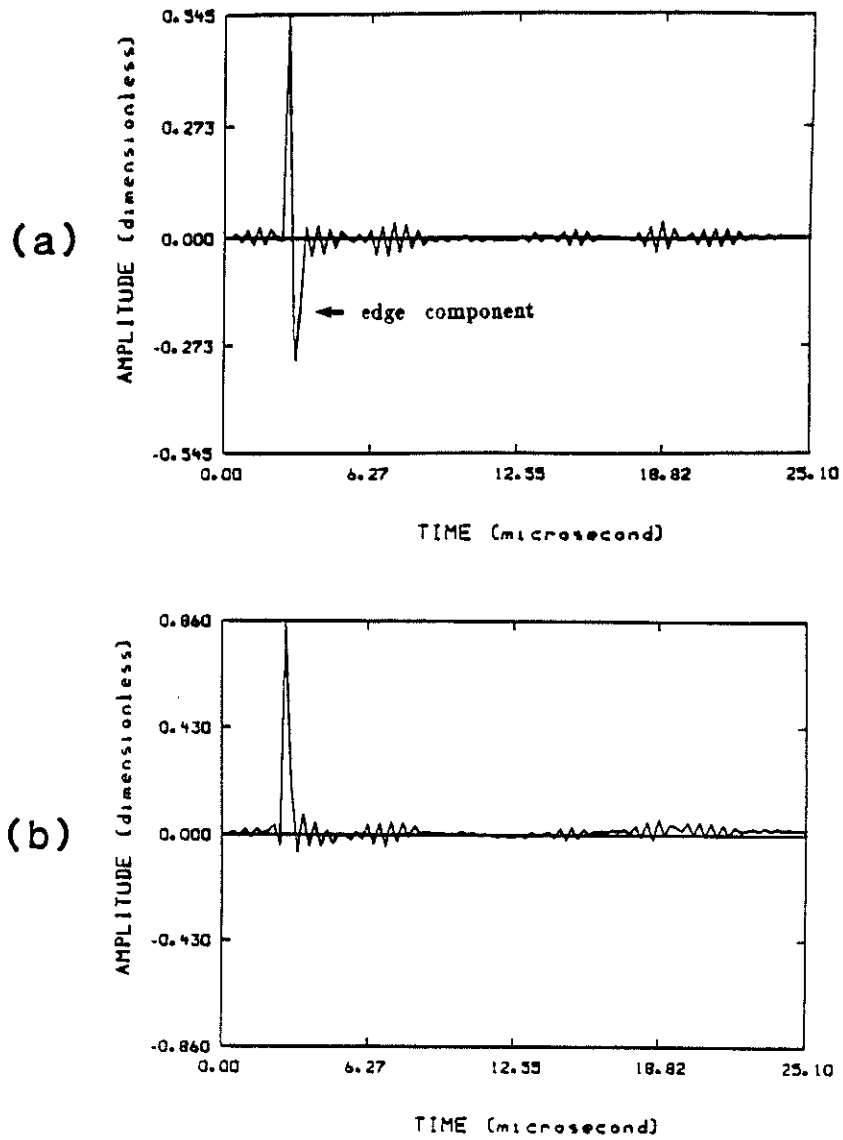| Medium	Density (g/cm³) (20°C)	Velocity (m/sec) (20°C)	Attenuation (cm⁻¹) (20°C)	
			1 MHz	10 MHz
Water	1.00	1440	0.001	0.04
Glycerol	1.26	1910	0.022	2.30
Mud (*water base*)	1.62	1480	to be measured	

Figure 9: (a) Recovered spatial impulse response in water. The edge wave is evident as seen from this figure. (b) A delta function like pulse obtained after making corrections for the diffraction effects.

relation

$$\alpha = -\frac{ln(amplitude)}{z_2 - z_1} \qquad (24)$$

where ln denotes taking the natural logarithm, and *amplitude* refers to amplitude of the transfer function. We use equation (23) to correct the edge wave effects and obtain the corrected transfer function. Figure 10 shows the attenuation coefficient obtained from the uncorrected (curve 1) and corrected (curve 2) transfer functions. Because the attenuation of water is negligible, one would expect α to be close to zero, as appears on curve 2. The corresponding impulse response is given in Figure 9b: the edge component is removed and the corrected response is effectively a delta function. As a conclusion, we can say that the corrections made for the diffraction effects are satisfactory.

Next we study glycerol, a moderately attenuative medium. To show the advantage of determining the attenuation operator when signals have extra arrivals, we record the first signal close to the source ($z_1 = 10mm$) so that the echoes that are reflected back and forth between the source and receiver surfaces arrive on the tail of the input signal (Figure 11a). The first signal with the echoes and a second one recorded at $z_2 = 80mm$ (Figure 11b) are then processed using the above procedure. The time domain and the frequency domain results are given in Figures 12 and 13, respectively. As seen from Figure 13, the input spectrum is affected by the echoes, and the attenuation obtained from the spectral ratio of the output with the input also exhibits this effect. However, the calculated impulse responses, both uncorrected and corrected for the diffraction effects (see Figure 12), are well separated from the echo effects. Also, as we can see from the same figure, the negative component of the uncorrected impulse response is largely reduced after its correction using equation (23). Windowing only the impulse responses, we obtain the smooth attenuation curves shown in Figure 13b. We see that, apart from the echo effects, the uncorrected attenuation curves calculated from the spectral ratio method and from the Wiener filtering are in general agreement, but they exhibit the important diffraction effects at low frequencies; whereas the corrected attenuation curve gives more reasonable results. Around 1 MHz, the measured attenuation is on the order of $0.03cm^{-1}$, in general agreement with the published result (Table 1). As frequency increases, the attenuation increases rapidly. With this tendency, one can expect α to reach the order of $2.3cm^{-1}$ at 10 MHz, as given by Table 1, although this is outside the frequency range of our measurement.

As the last example, we study a highly attenuative medium: an argillaceous mud. The typical received near and far source signals in mud have already been shown in Figure 1a, where the input and the output are at $z_1 = 34mm$ and $z_2 = 94mm$, respectively. The impulse response derived from them is shown in Figure 14 (the uncorrected curve). Although the effects of attenuation are dominant, the uncorrected impulse response still exhibits a broad, slightly negative tail, which reveals the presence of the edge effect. This effect is corrected using equation (23). Compared with the uncorrected response, the corrected response is broadened (low frequency content restored) and its amplitude is
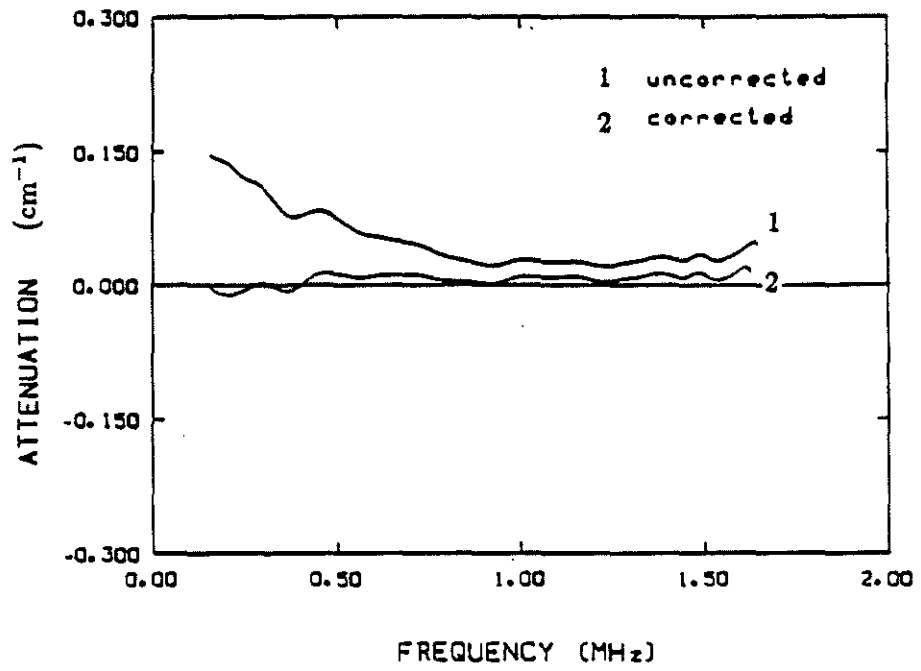
Figure 10: The uncorrected and corrected attenuation coefficients of water. Note that the corresponding wave spectra were shown in Figure 7.
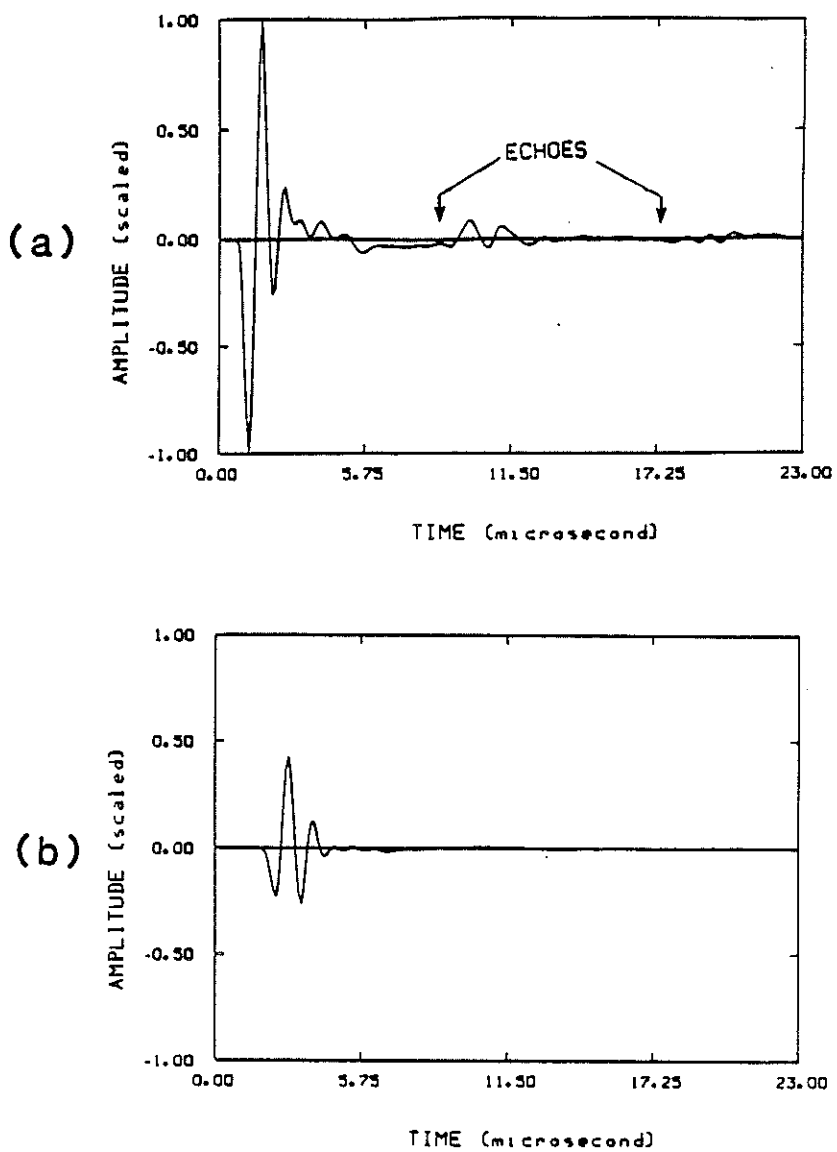
Tang et al.

(a)

(b)

Figure 11: (a) Input signal (received at $z_1 = 10mm$ in glycerol) with echoes. (b) Output signal received at $z_2 = 80mm$.
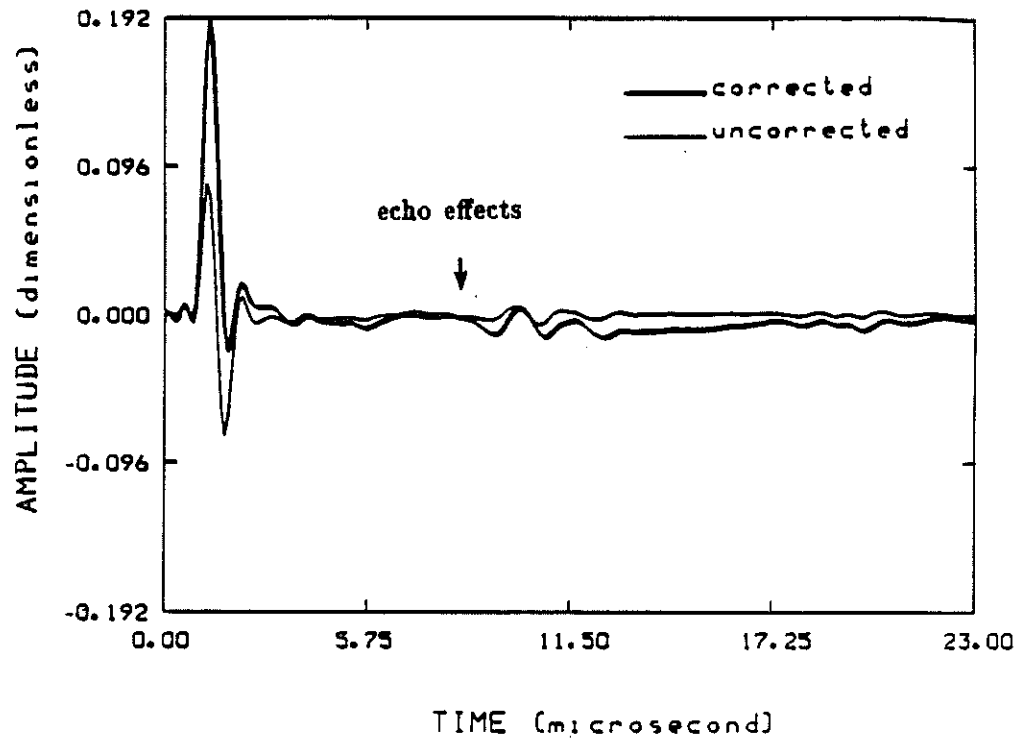
Figure 12: The uncorrected and corrected impulse responses of glycerol. Note that the echo effects are separated from the impulses.
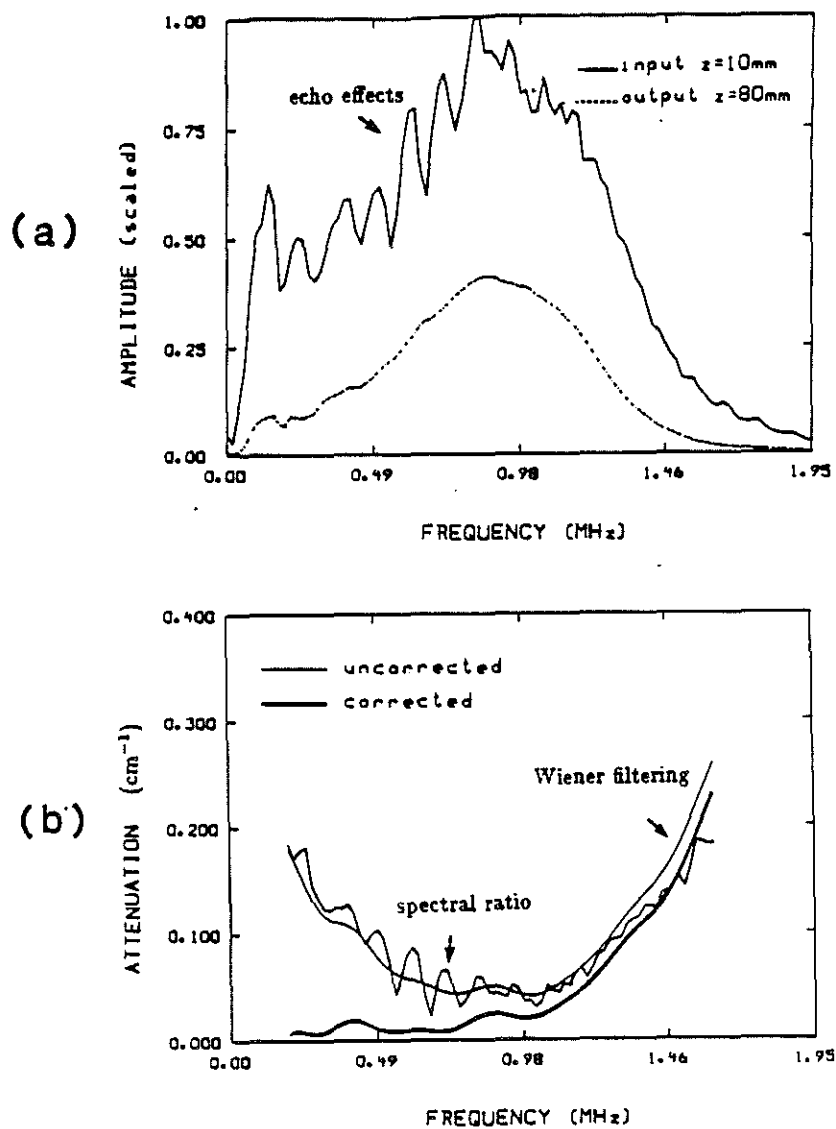
Figure 13: (a) Wave spectra of the input and output signals shown in Figure 11. The input spectrum exhibits the effects due to the echoes in Figure 11a. (b) Comparison of attenuation coefficients. The attenuation curve calculated using the spectral ratio shows the echo effects. The thin curve obtained using Wiener filtering is corrected for the diffraction effects to give the attenuation coefficient of glycerol (darker curve).
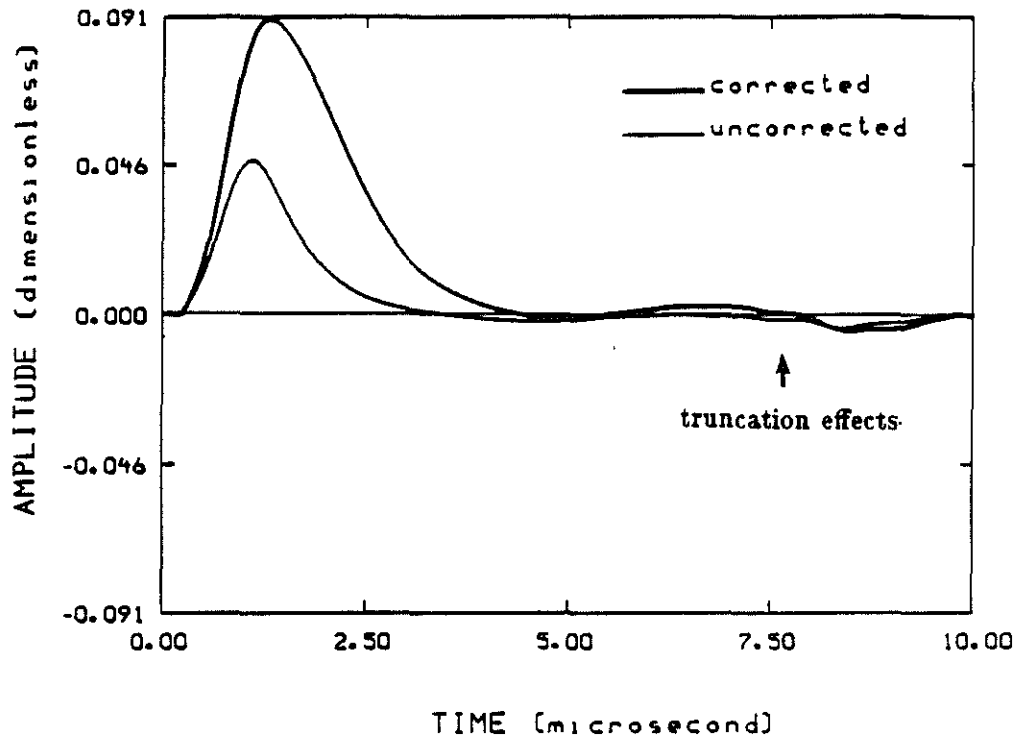
Figure 14: Comparison of the corrected and uncorrected impulse response of mud. The arrow points to the onset of the effects due to the truncation of the input and output signals.

recovered. Also, one may notice the fluctuation following the impulse responses. This is due to the truncation effects of the signals, and can be removed by windowing only the impulse responses. Figure 15b shows the attenuation coefficients obtained from the uncorrected response, the spectral ratio method (the two spectra used are shown in Figure 15a), and the corrected response. Obviously, attenuation curves obtained using Wiener filtering are smoother than that obtained using the spectral ratio method, and because the truncation effects are removed from the impulse responses, their attenuation curves are still valid in a higher frequency range, where the output spectrum (Figure 15a) has very little energy. Also, we notice that the uncorrected curve is different from the corrected one at the low frequencies because of the diffraction effects. The corrected attenuation coefficient is roughly proportional to frequency, suggesting a constant Q behavior of the mud medium. (Hovem (1980) gave an explanation of the $\alpha \propto \omega^1$ behavior by taking into account the grain size distribution in a modified suspension theory). Thus, the quality factor Q is derived from the slope γ of the attenuation curve via the following relation (Toksöz et al., 1978)

$$Q = \frac{\pi}{\gamma c} \tag{25}$$

For the mud, we find $Q = 31 \pm 2$ (the error indicated is obtained through calculations for a set of different separations). Without any correction, we find Q about 40, and because the diffraction effects vary with distance, the uncorrected Q values range from 35 to 45.

CONCLUSIONS

The main purpose of this study was to investigate a method of measuring intrinsic attenuation. We showed that the direct measurement of an attenuation operator in the time domain is an effective approach. The attenuation operator can be calculated using Wiener filtering deconvolution. Because Wiener filter is often unstable, damped least-squares has been used to stabilize the computation. Using the perturbation method, we have calculated the time domain corrections for the effects due to the addition of the damping constant.

It has also been shown that it is possible to separate the intrinsic attenuation effects from the effects due to extra arrivals by windowing the attenuation effects on the calculated attenuation operator. This is possible when the signals used for the deconvolution are more significant than extra arrivals, and the duration of the attenuation operator is short compared to the arrival time difference between the signal itself and the extra arrivals.

We showed that the diffraction effects of a source of finite size can seriously affect the results of attenuation measurements. These effects can be corrected by equating
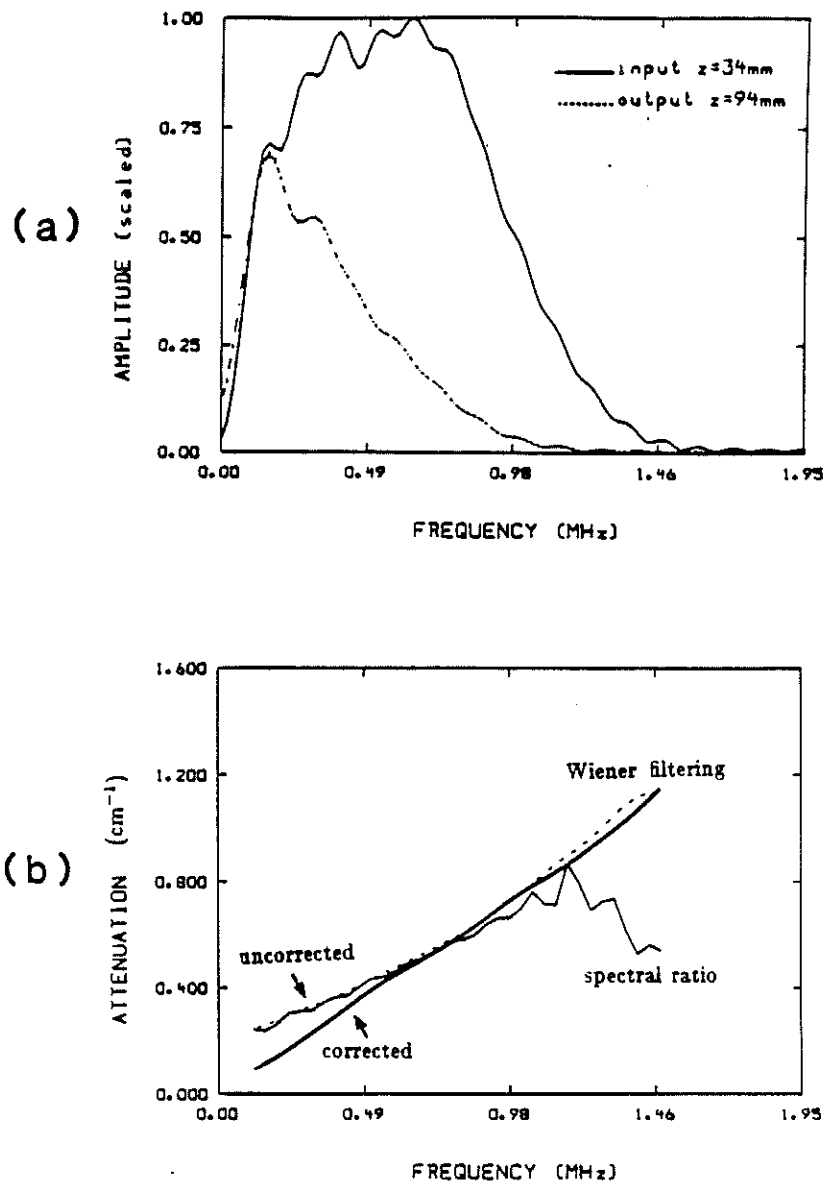
Figure 15: (a) Wave spectra of the input and output signals received at $z_1 = 34mm$ and $z_2 = 94mm$ in mud, respectively. (b) Comparison of the uncorrected and corrected attenuation coefficients of mud.

the received signal to the average pressure over the receiver surface. Measurements in water, glycerol, and mud gave reasonable results and showed that the techniques used here and the corresponding corrections are satisfactory, thus offering a useful tool for the measurement of attenuation.

ACKNOWLEDGEMENTS

REFERENCES

Aki, K., and Richards, P., 1980, Quantitative Seismology–Theory and Methods, v.2; Freeman, San Francisco.

Bass, R., 1958, Diffraction effects in the ultrasonic field of a piston source; J. Acoust. Soc. Am., 30, 602–605.

Harris, G.R., 1981, Review of transient field theory for a baffled planar piston; J. Acoust. Soc. Am., 70, 10–20.

Hovem, J.M., 1980, Viscous attenuation of sound in suspensions and high porosity sediments; J. Acoust. Soc. Am., 67, 1559–1563.

Gitis, M.B., and Khimunin, A.S., 1969, Diffraction effects in ultrasonic measurements; Sov. Phys. Acoust., 14, 413–431.

Kjartansson, E., 1979, Constant Q wave propagation and attenuation; J. Geophys. Res., 84, 4734–4748.

Peacock, K.L., and Treitel, S., 1969, Predictive deconvolution: theory and practice; Geophysics, 34, 155–169.

Richardson, E.G., 1962, Ultrasonic Physics; Elsevier, New York.

Taylor, S.R., and Toksöz, M.N., 1982, Measurement of interstation phase and group velocity and Q using Wiener filtering; Bull. Seism. Soc. Am., 72, 73–91.

Toksöz, M.N., Johnston, D.H., and Timur, A., 1978, Attenuation of seismic waves in dry and saturated rocks: I. Laboratory measurement; Geophysics, 44, 681–690.

Wiener, N., 1949, Time Series; M.I.T. Press, Cambridge, Mass.

Williams, A.O., Jr., 1951, The piston source at high frequencies; J. Acoust. Soc. Am., 23, 1–6.